RESEARCH ARTICLE

Figures and figure supplements

Diffusion MRS tracks distinct trajectories of neuronal development in the cerebellum and thalamus of rat neonates

Clémence Ligneul *et al*.

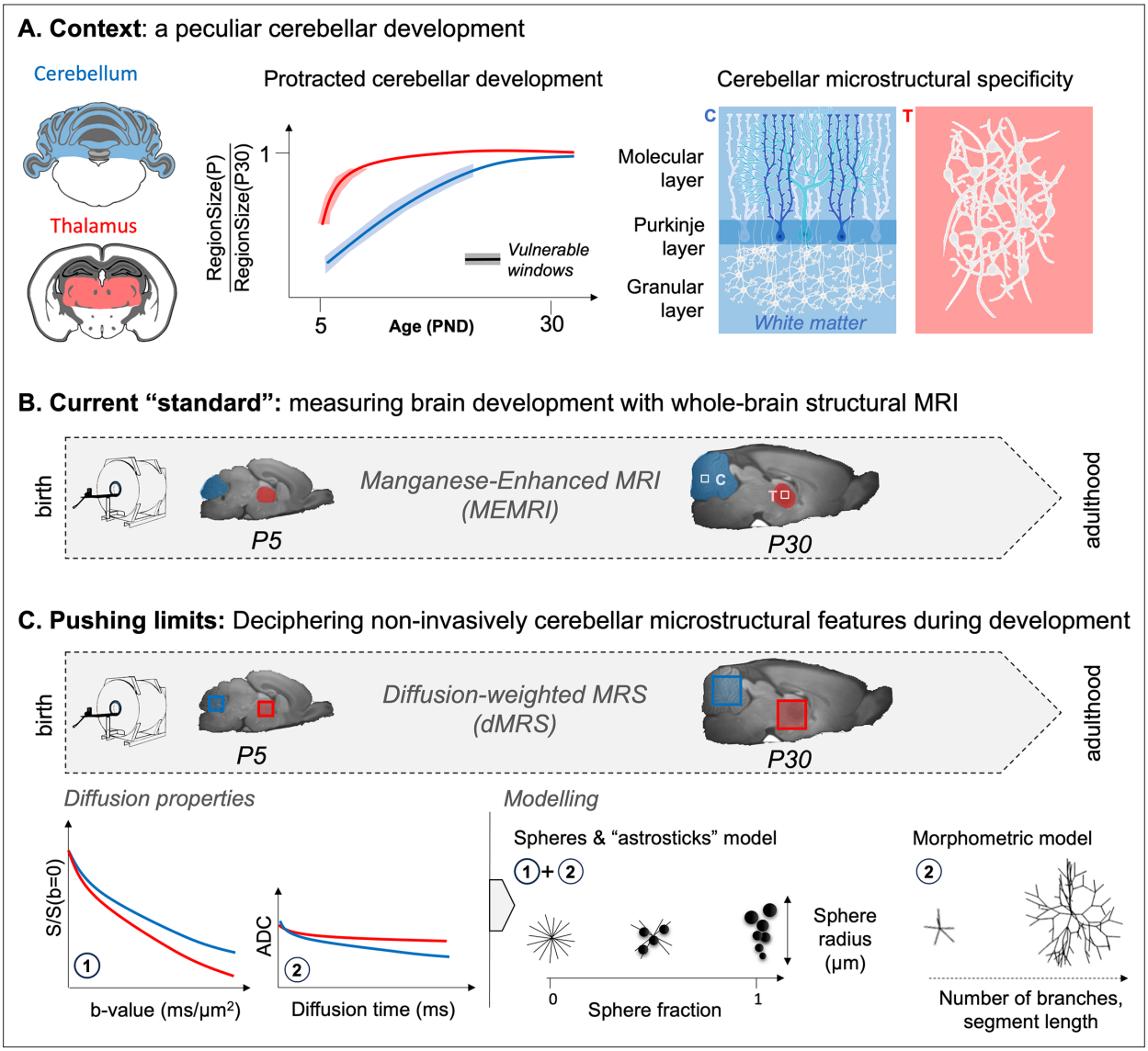

Figure 1. Overview of the rationale of the study. (**A**) Context: the cerebellum exhibits protracted growth compared to other brain regions (e.g. thalamus), making it a particularly vulnerable region for neurodevelopmental disorders. Its specific microstructural organisation (i.e. layered with Purkinje cells and granular cells) changes between birth and adulthood. (**B**) The current 'standard' is to probe regional growth with manganese-enhanced MRI (MEMRI). However, it is not sensitive to the underlying microstructural changes. (**C**) Pushing limits: diffusion-weighted MRS (dMRS) can potentially assess cell-specific microstructural changes in given regions during development. Different measures of metabolites' diffusion properties (apparent diffusion coefficient [ADC] at long diffusion times, signal attenuation [S] at high diffusion weighting, b-values) can be interpreted with biophysical modelling and help characterise the nature of the microstructural changes.

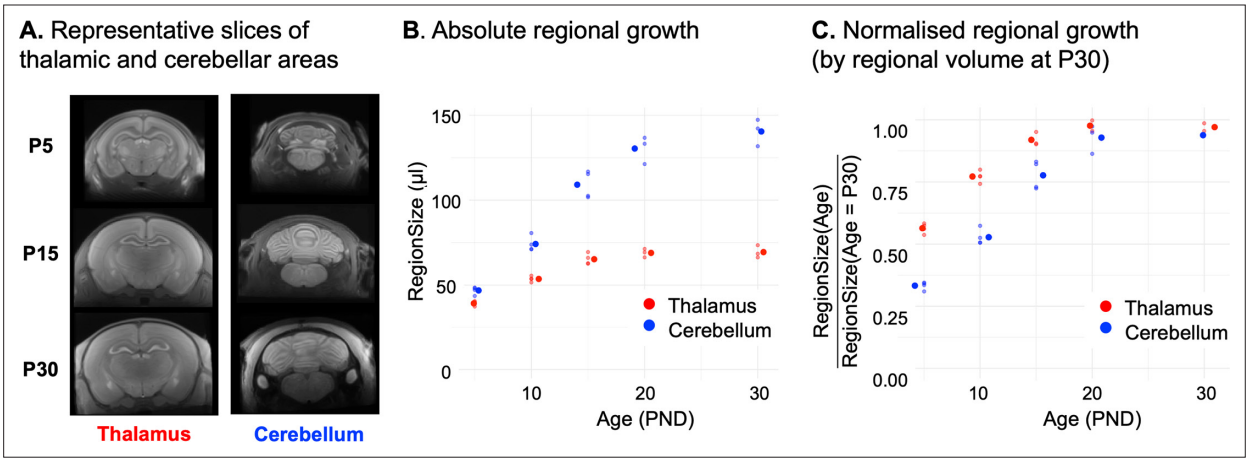

Figure 2. Manganese-enhanced MRI confirms protracted cerebellar growth in rat pups. (**A**) Representative slices around the thalamus and cerebellum of non-linearly averaged images acquired at postnatal day 5 (P5), P15, and P30. (**B**) Absolute volumetric changes are shown for the segmented thalamus and cerebellum. Large dots correspond to the mean and small dots to individual data points. (**C**) Normalised volumetric changes. Volume at each age is normalised by the P30 volume. Large dots correspond to the mean and small dots to individual data points.

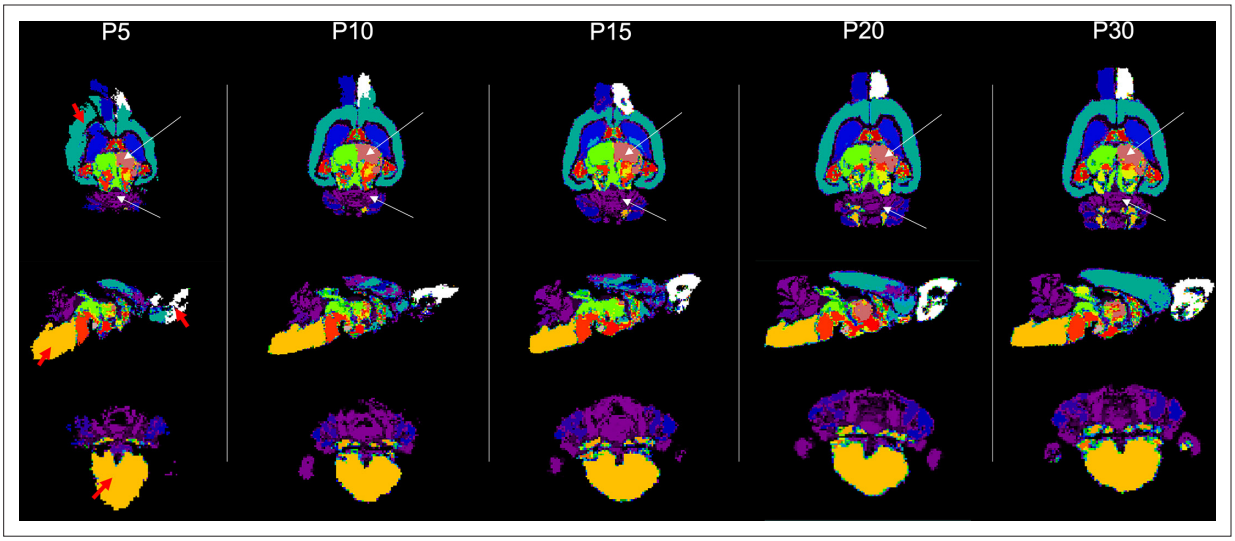

Figure 2—figure supplement 1. Representative segmented atlases at each time point. The reference atlas used for the longitudinal analysis is a postnatal day 15 (P15)-Fischer-derived atlas. The atlas was derived from a P15-P20 registration (using a P20-Fischer-derived atlas, itself derived from a P20-P30 registration using the original Fischer atlas). White arrows point at the thalamus and cerebellum segmentations. Red arrows point at the major registration artefacts.

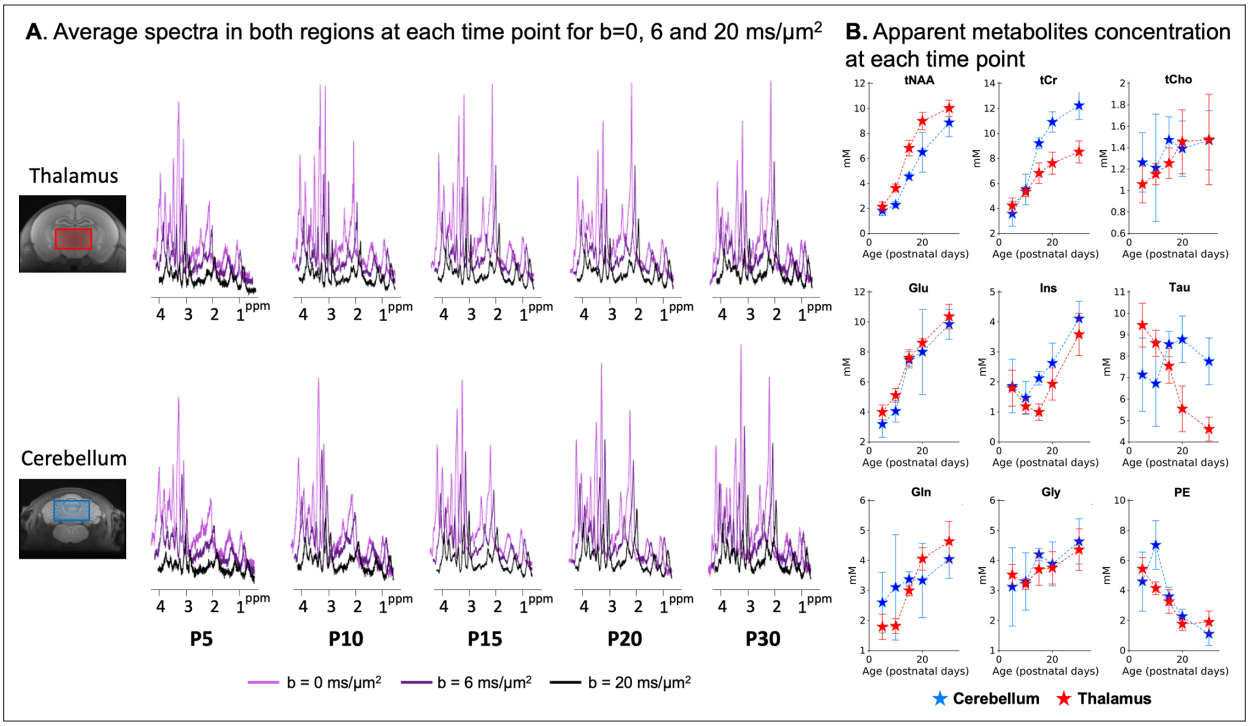

Figure 3. Metabolic profile changes postnatally. (**A**) Spectra were binned by time point, region, and b-value, and averaged after phase and frequency correction. The SNR is clearly lower at postnatal day 5 (P5)/P10 in both regions: the voxel is about half of the P30 voxel size, and more animals were outliers. The SNR is also lower at P30: the rat size was slightly too big for the mouse cryoprobe at this age, so the skull is not at the top of the probe and the sensitivity is suboptimal. (**B**) Individual spectra at b=0.035 ms/μm^2 were quantified with LCModel, and absolute metabolite concentrations were normalised by the water content and levelled to get Signal(tCr,P30)/Signal(water,P30)~8 in the thalamus. See ***Figure 3—figure supplement 1*** for a comparison with normalisation by MM.

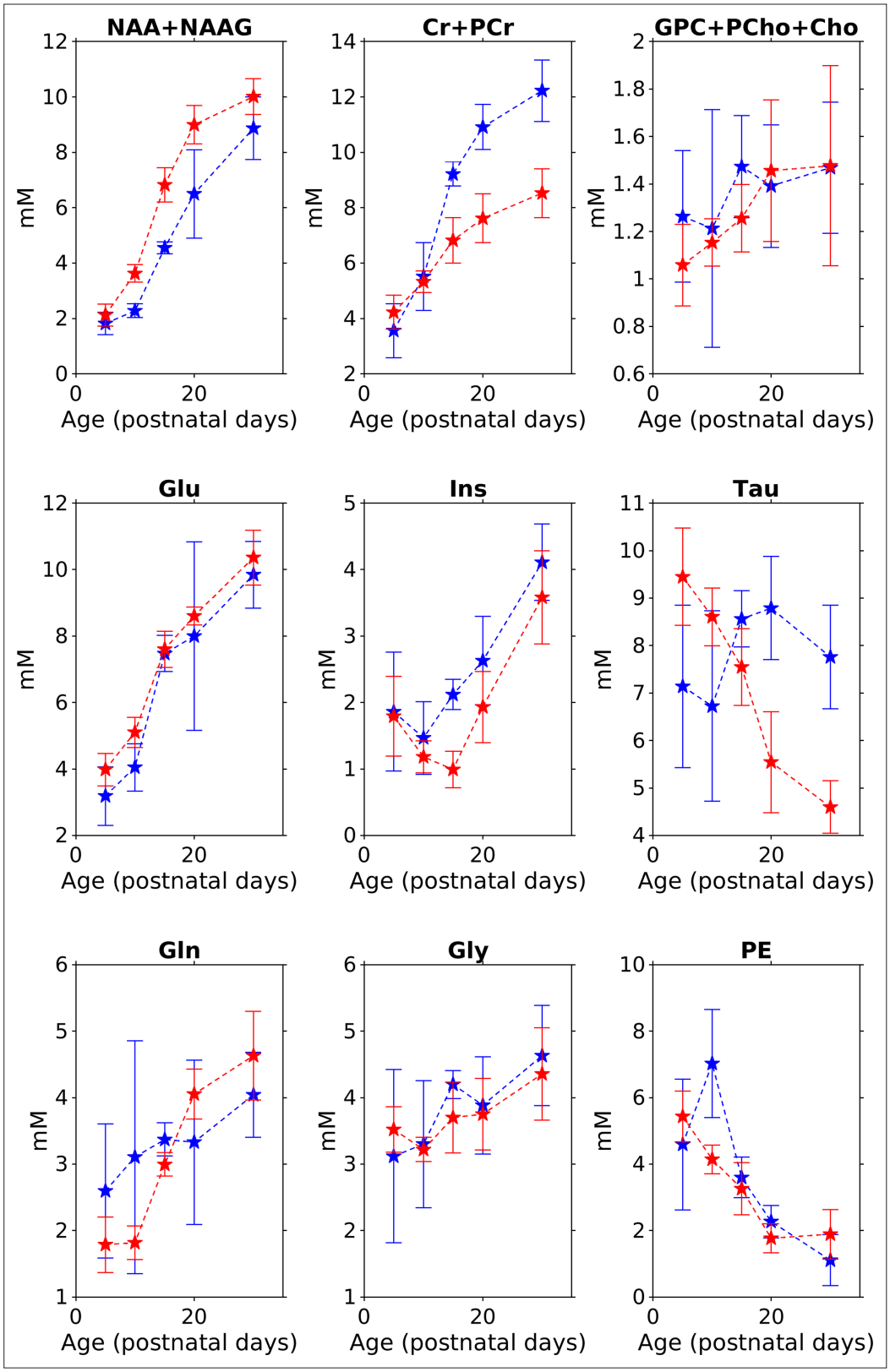

Figure 3—figure supplement 1. Cerebellar (blue) and thalamic (red) metabolic changes with age. This figure complements ***Figure 3***. Spectra at b=0.035 ms/μm^2 and TM = 100 ms were quantified with LCModel, and absolute metabolite concentrations were normalised by either the absolute voxel water signal (white columns) or the absolute voxel macromolecular concentration (grey columns).

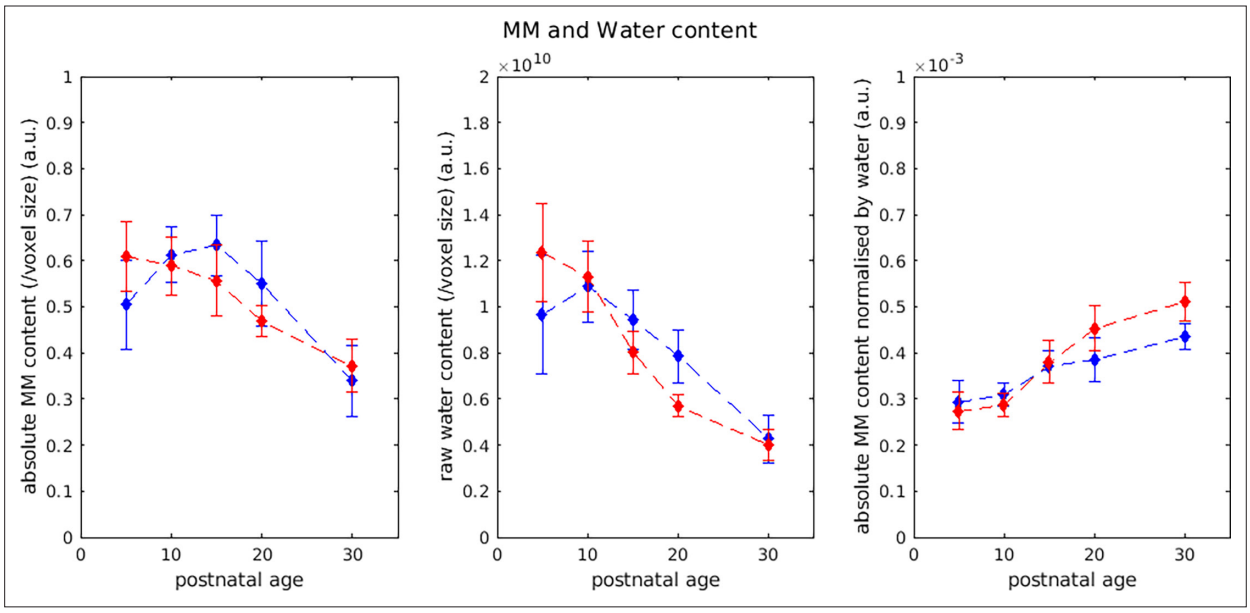

Figure 3—figure supplement 2. Cerebellar (blue) and thalamic (red) molecular and water content changes with age. Absolute MM content in the voxel normalised by voxel size (left), raw water content normalised by voxel size (middle), and MM content normalised by water content (right). All in arbitrary units.

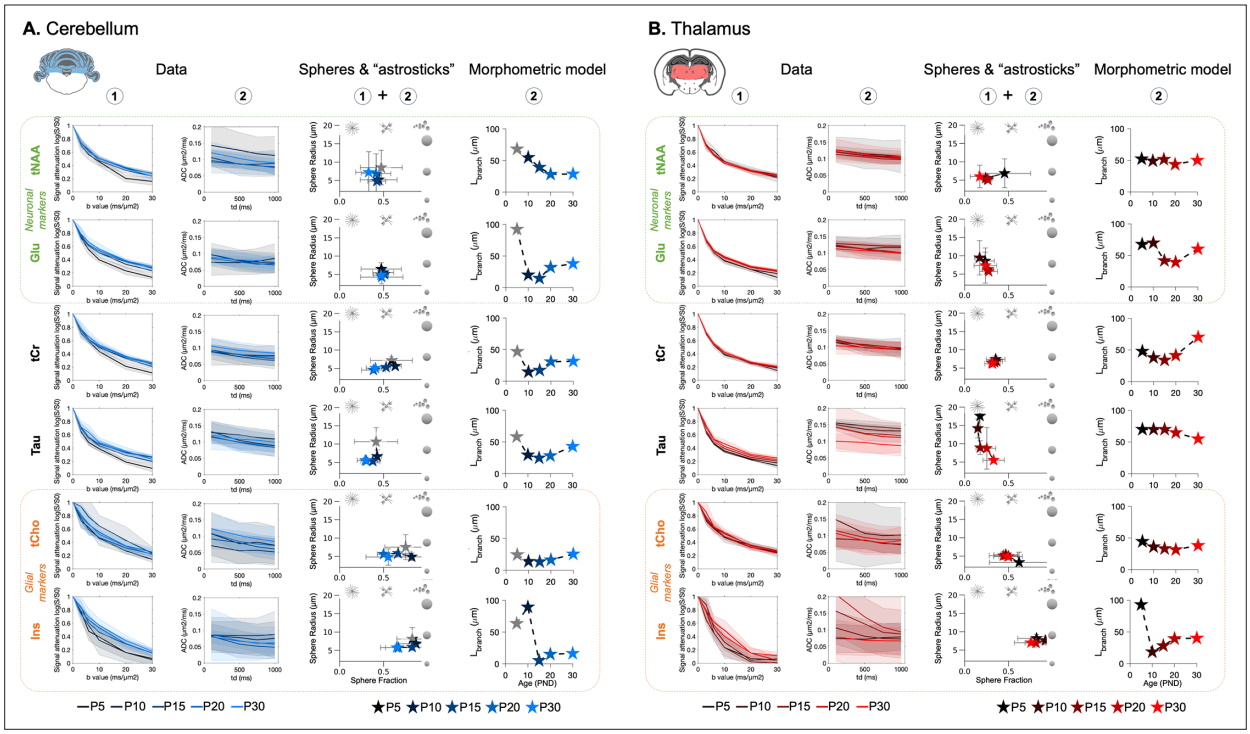

Figure 4. Biophysical modelling issued from metabolites diffusion properties shows differential developmental trajectories in the cerebellum (**A**) and in the thalamus (**B**). The first column (**A, B**) reports the signal attenuation as a function of b-value at TM = 100 ms, and the second column reports the apparent diffusion coefficient (ADC) varying with diffusion time. Shadowed error bars represent the standard deviations. Modelling results from the spheres+'astrosticks' model are reported in the third column (**A, B**). Postnatal day 5 (P5) is shaded in the cerebellum due to possible motion artefact. The parameter space (sphere fraction, sphere radius) is displayed. Error bars represent the standard deviations. L_{length}, modelling output from the morphometric model, is shown in the fourth column (**A, B**). P5 is shaded in the cerebellum due to possible motion artefact.

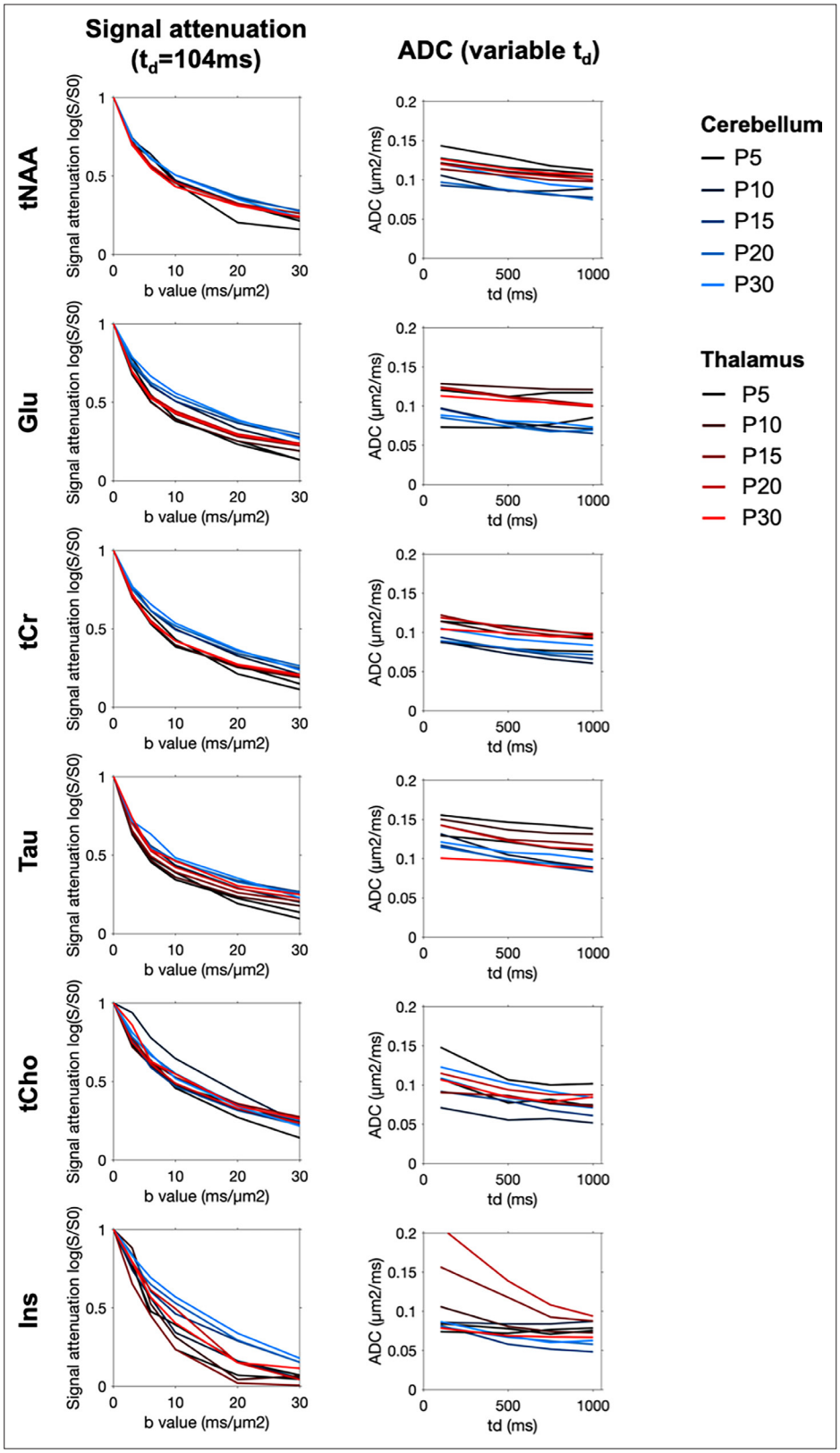

Figure 4—figure supplement 1. Visual comparison of diffusion properties between regions and at each time point.

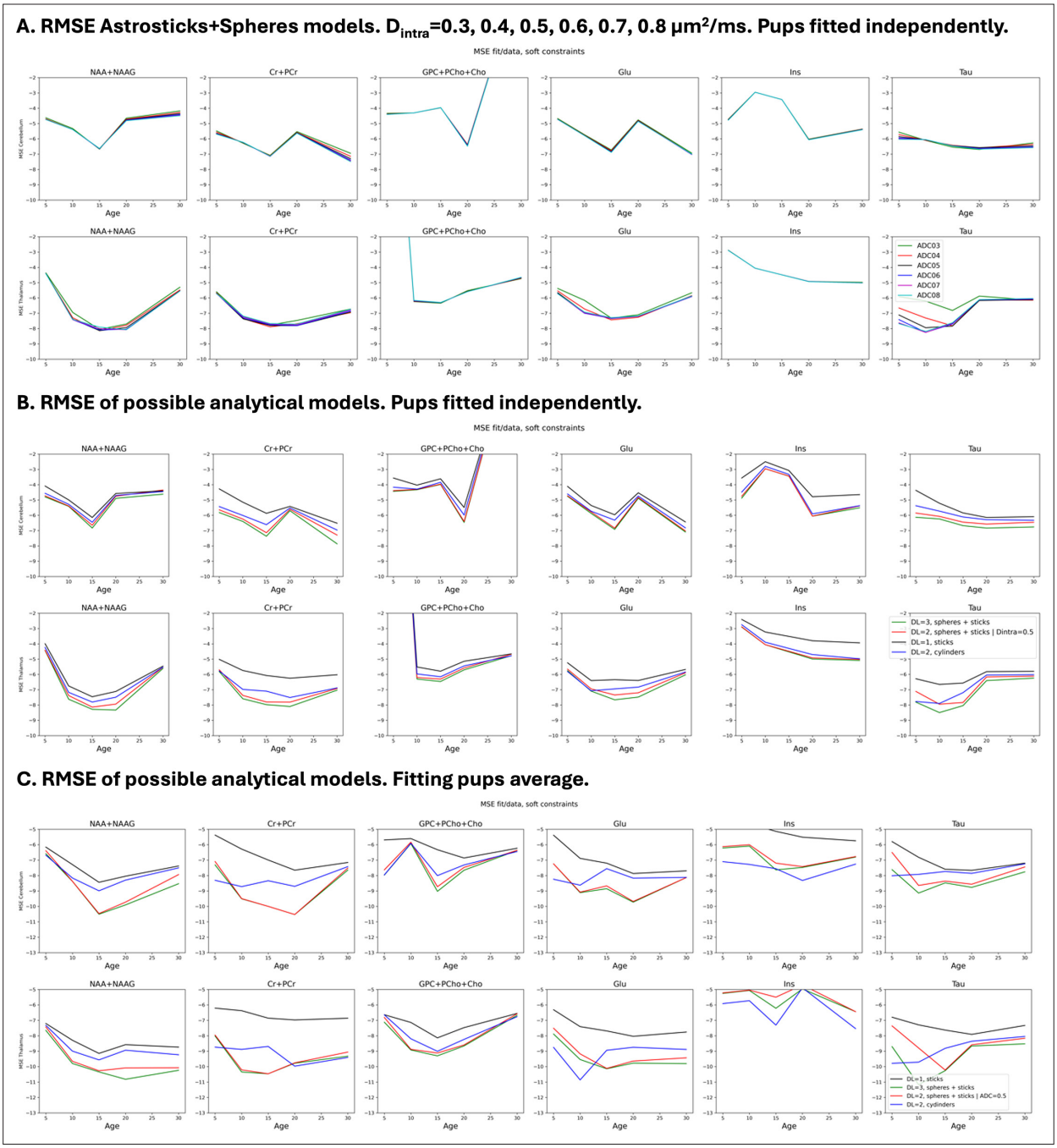

Figure 4—figure supplement 2. Analytical model residuals. Root mean square error (RMSE) computed from the results of the analytical modelling ('astrosticks and spheres'). The logarithm is displayed for visualisation: log(residuals = rmse(model fit – data)). (**A**) RMSE of the 'astrosticks'+spheres model with D_{intra} fixed. D_{intra} values probed = 0.3, 0.4, 0.5, 0.6, 0.7, 0.8 µm²/ms. The mean value over all pups is displayed at each time point in each region (neonates fitted independently). (**B**) RMSE computed for the 4 analytical models assessed: 'astrosticks' (DL = 1), 'astrocylinders' (DL = 2), 'astrosticks + spheres' (DL = 3), 'astrosticks + spheres' – fixed D_{intra}. The mean RMSE value over all pups is displayed at each time point in each region (neonates fitted independently). (**C**) RMSE computed from the averaged data at each time point in each region for the 4 analytical models assessed: 'astrosticks' (DL = 1), 'astrocylinders' (DL = 2), 'astrosticks + spheres' (DL = 3), 'astrosticks + spheres' – fixed D_{intra} (neonates pooled by age and region and average fitted).

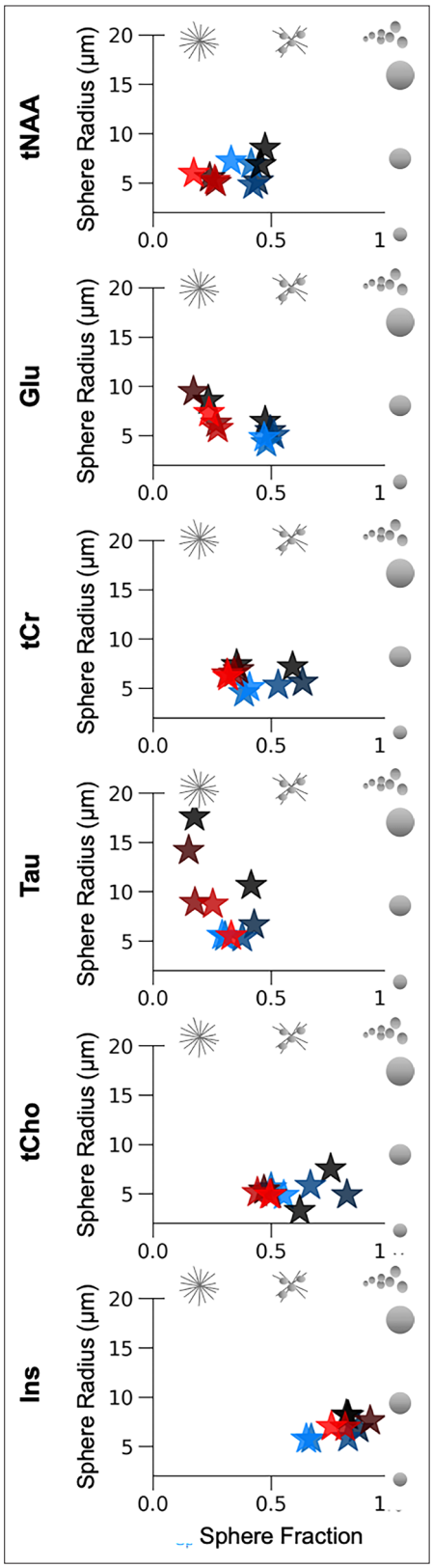

Figure 4—figure supplement 3. Visual comparison of the parameter space (sphere fraction, sphere radius) between the cerebellum and the thalamus at each time point for the 'astrosticks + spheres' model (D_{intra} =0.5 $\mu m^2/ms$).

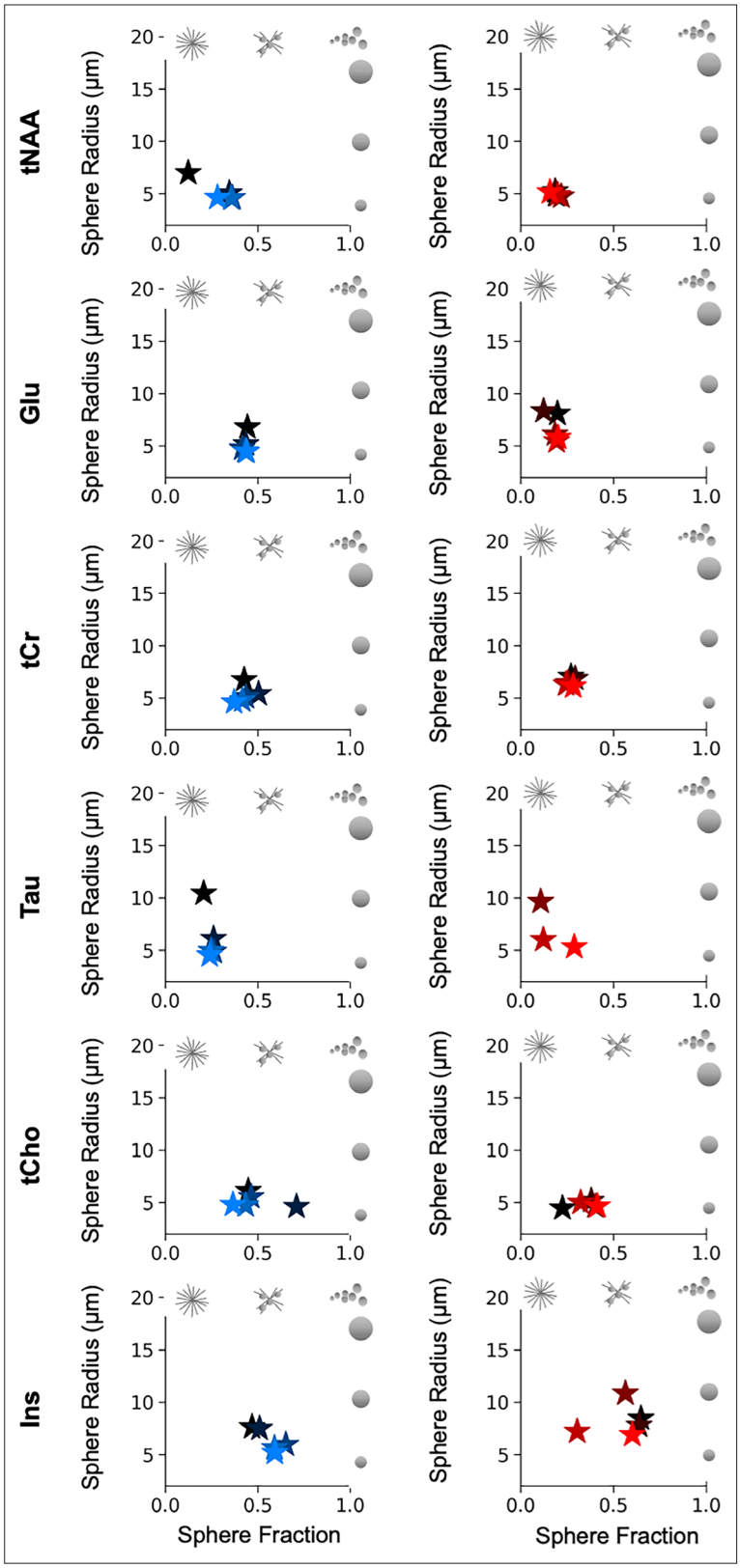

Figure 4—figure supplement 4. Parameter space (sphere fraction, sphere radius) between the cerebellum and the thalamus at each time point for the 'astrosticks + spheres' model (D_{intra} =0.5 µm^2/ms) on averaged neonates.

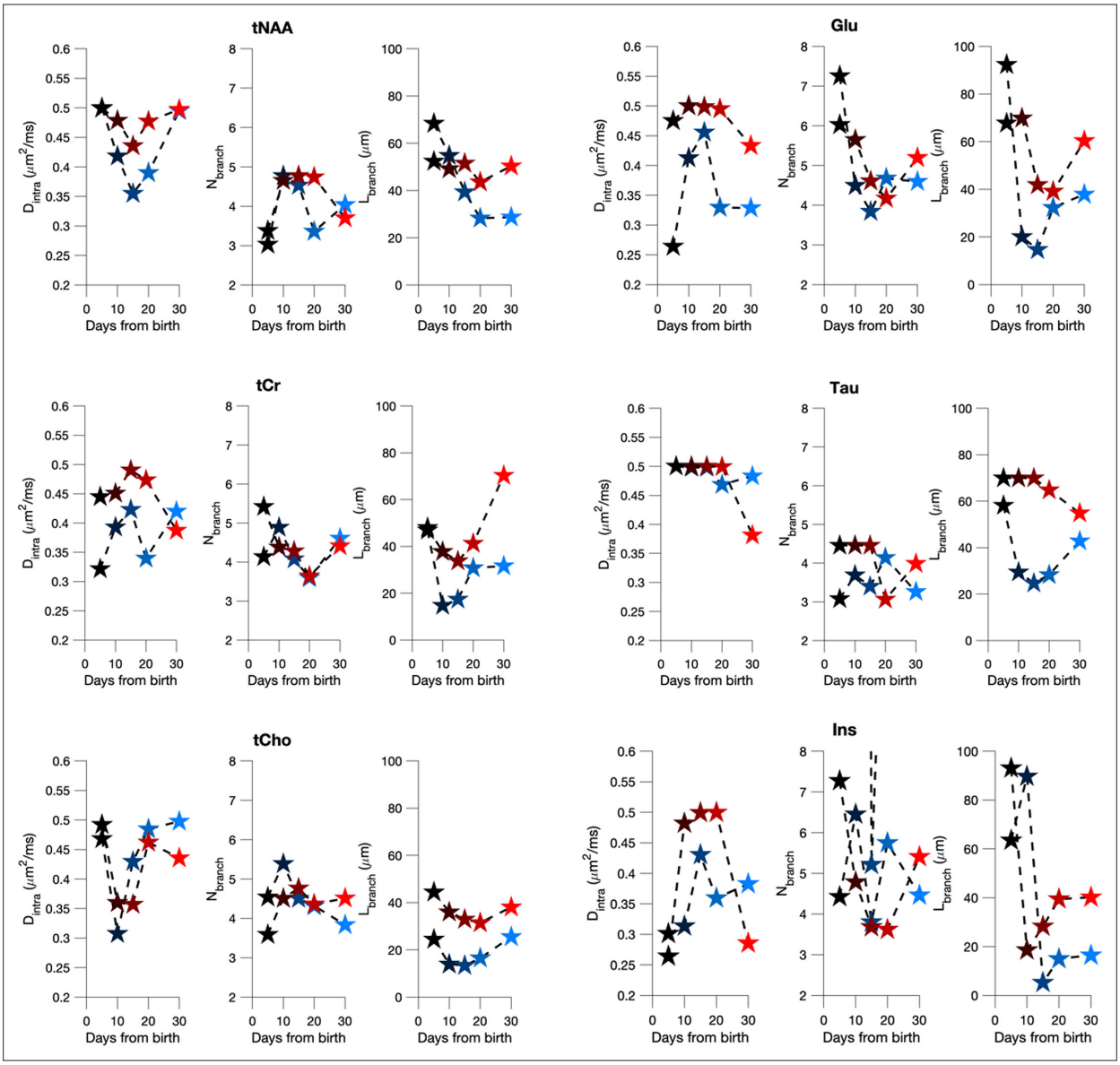

Figure 4—figure supplement 5. Visual regional comparison of parameters estimated from the morphometric model. Estimations of D_{intra}, N_{branch}, $L_{segment}$ are shown for the six metabolites in two regions.

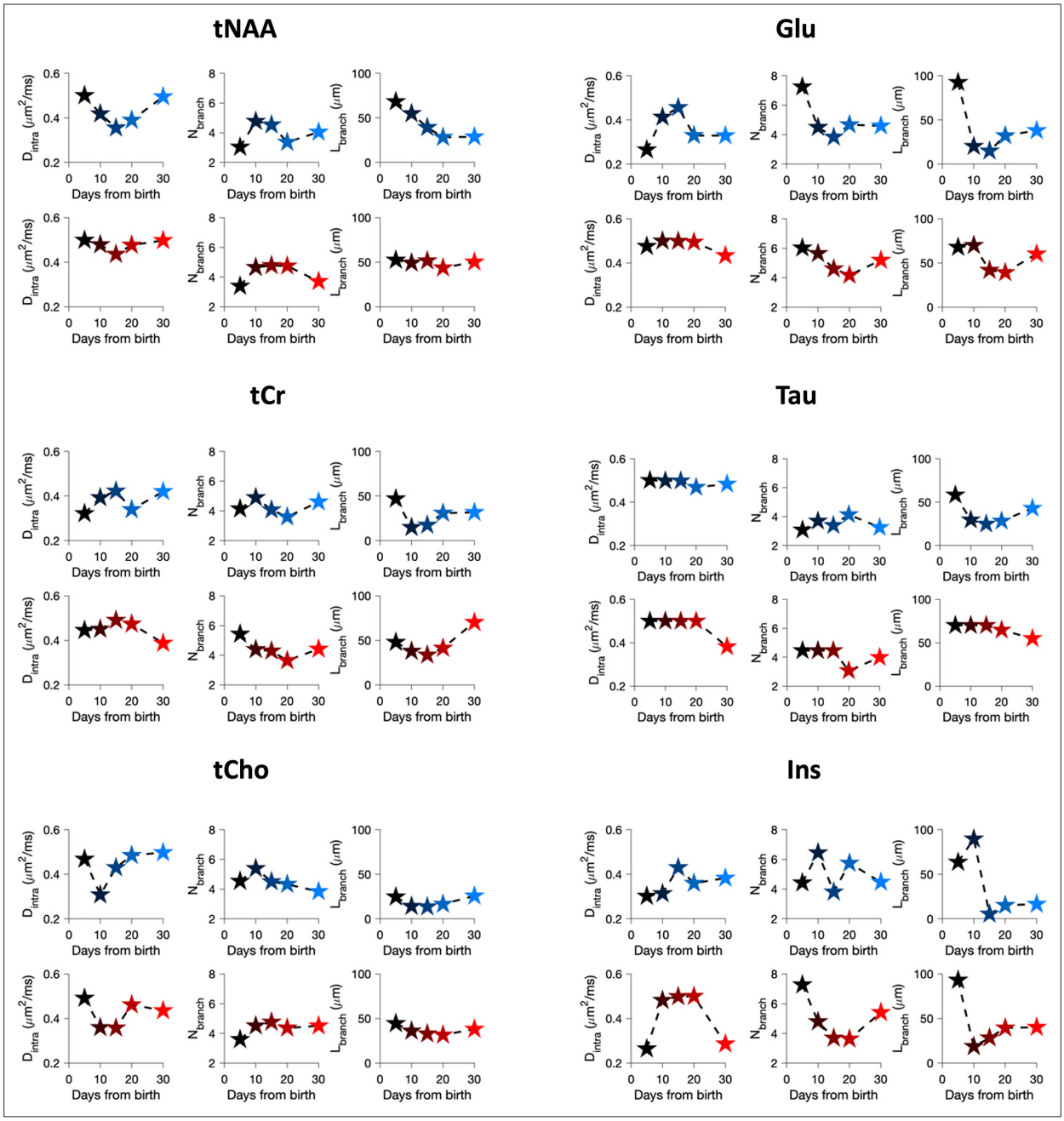

Figure 4—figure supplement 6. Estimations from the morphometric model of D_{intra}, N_{branch}, $L_{segment}$ are shown for the six metabolites in two regions.

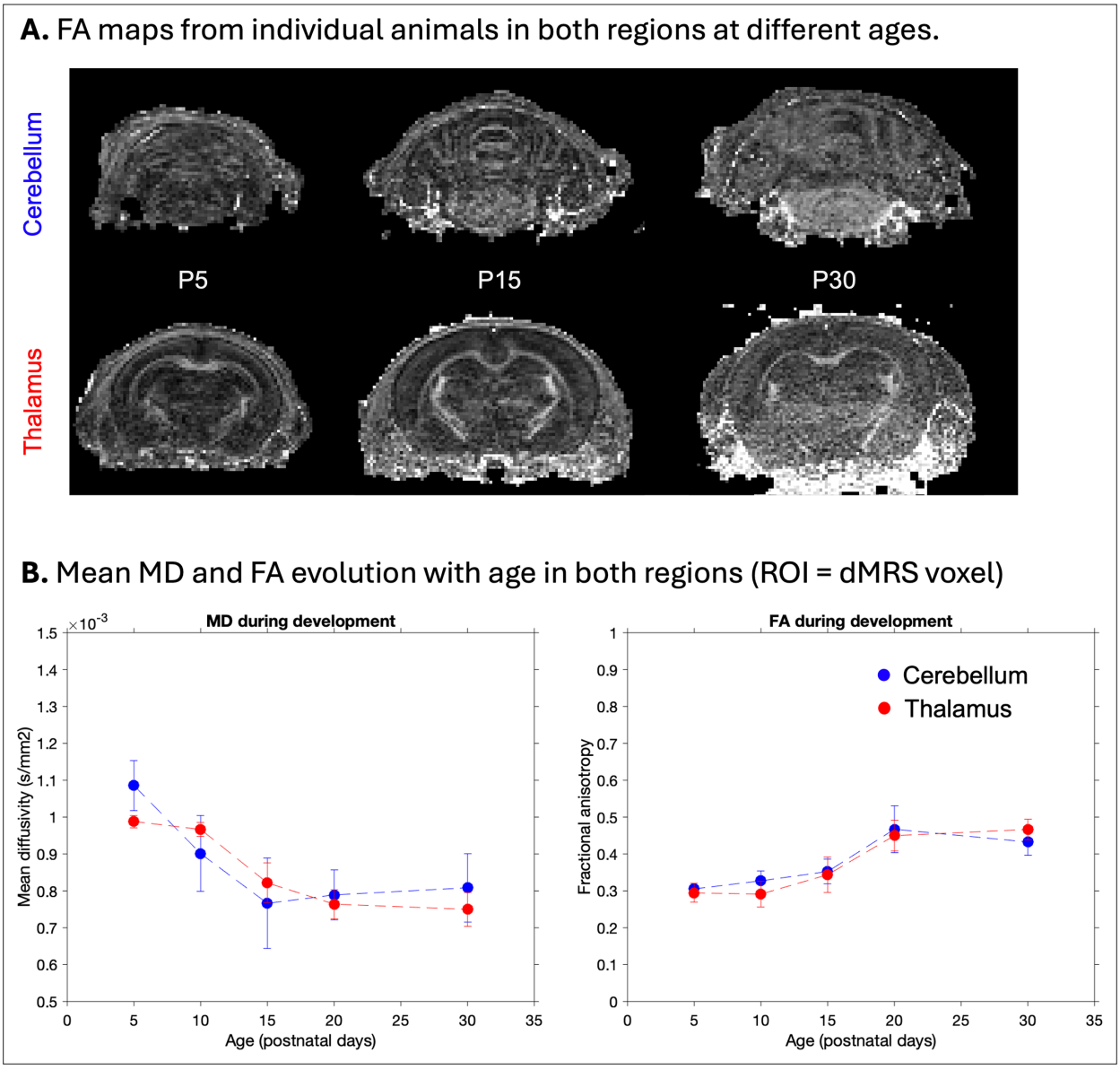

Figure 4—figure supplement 7. DTI results in the cerebellum and thalamus. (**A**) Representative fractional anisotropy (FA) maps at postnatal day 5 (P5), P15, and P30 in both regions. Images are not at scale. The image quality is particularly poor at P30, where the ghosting artefact in the ventral part of the brain appears in almost all images (poor FOV calibration). (**B**) Mean MD and FA evolution with age in both regions. The MD and FA values were averaged over the diffusion-weighted magnetic resonance spectroscopy (dMRS) voxel projected onto the maps. Values come from 12 animals (6 for each region). Given the poor image quality, we refrain from drawing conclusions from these results, but we include them in the Figure Supplement Information for thoroughness. *Methods*: SE-EPI sequence (4 segments, TR = 2.5 s, TE = 23.5 ms, resolution: 200 µm isotropic, 30 directions, b=1000 s/mm^2, 3 b=0 images, ∂=2.5 ms, Δ=10 ms).

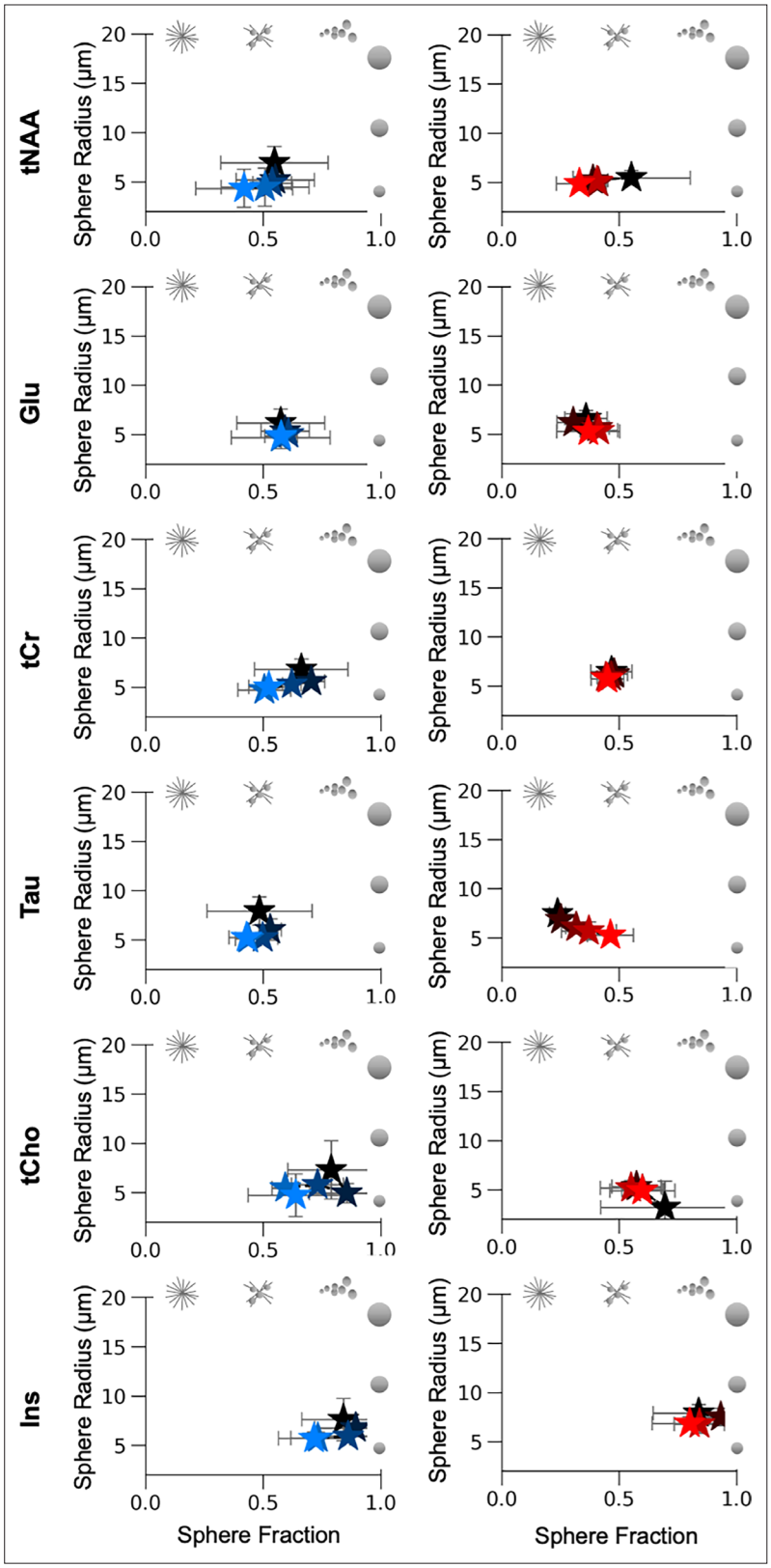

Figure 4—figure supplement 8. Parameter space (sphere fraction, sphere radius) between the cerebellum and the thalamus at each time point for the 'astrosticks + spheres' model (D_{intra} =0.7 μm^2/ms).

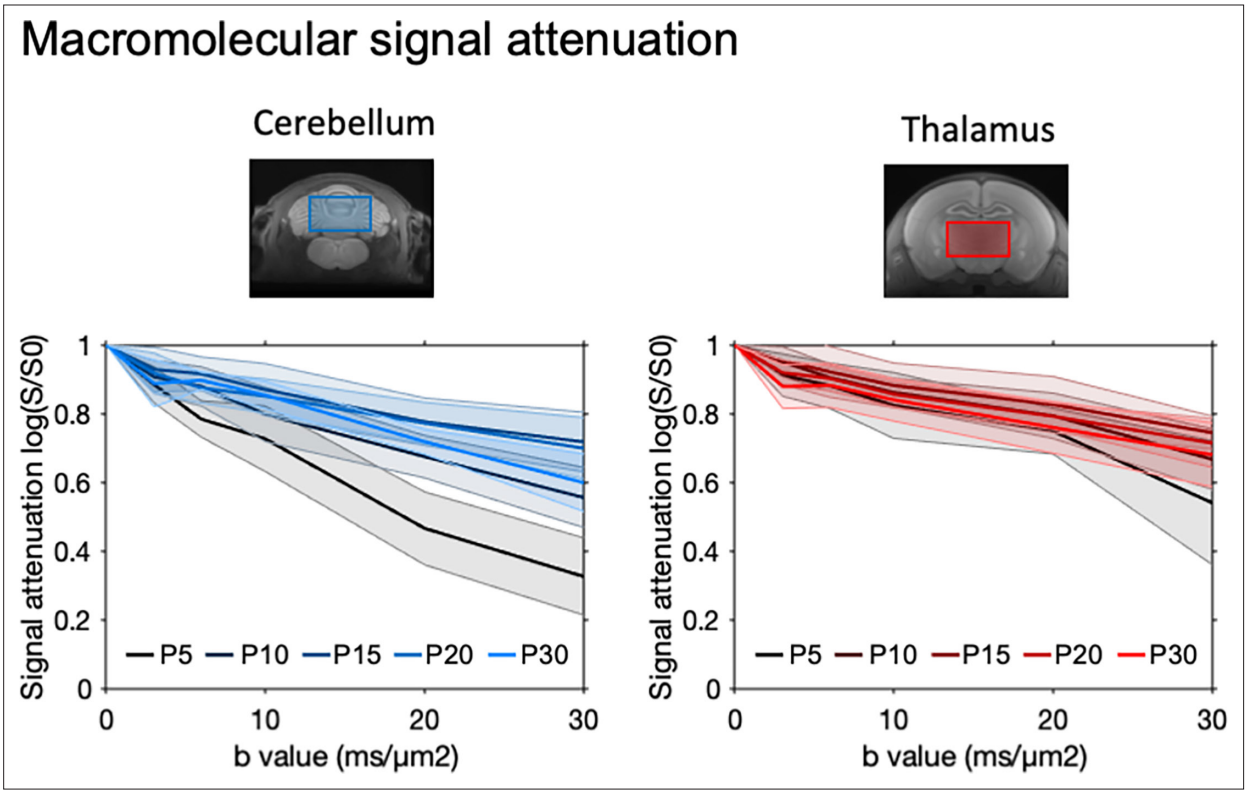

Figure 4—figure supplement 9. Average macromolecule signal attenuation in both regions at each time point coming from the LCModel fit. The macromolecule signal attenuation is abnormally strong in the cerebellum at postnatal day 5 (P5) (black line, left). This underlines a residual motion artefact that could not be corrected during processing. The shaded error bars represent the standard deviation from the mean.

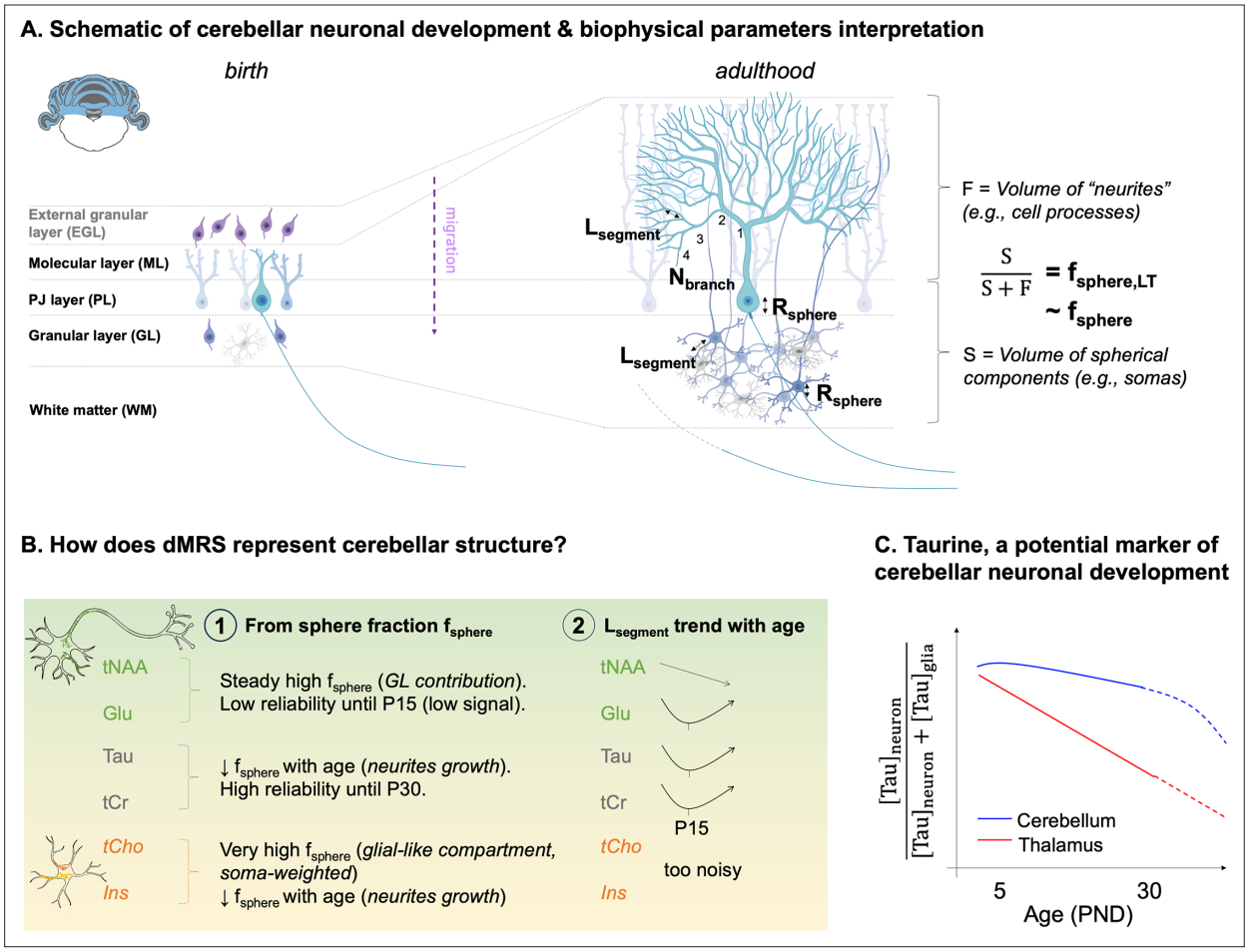

Figure 5. The biophysical parameters are interpreted based on the cerebellar microstructural development and main results are summarised. Italic font corresponds to possible interpretations. (**A**) Schematic of cerebellar neuronal development and biophysical modelling parameters interpretation. $L_{segment}$ is interpreted as the distance between two branches of the dendritic tree, N_{Branch} as the number of embranchments. The sphere radius R_{sphere} is interpreted as the average soma radius (i.e. granule and Purkinje cells). $f_{sphere,LT}$ represents the ratio of cerebellar layer thicknesses between the layers rich in sphere-like cell components (e.g. somas in the I/EGL, GL, and PL) and the layers rich in fibrous cell components (e.g. cell processes or 'neurite' in the ML). $f_{sphere,LT}$ can be seen as a rough approximation of f_{sphere} and is inversely related to the dendritic tree growth, see ***Supplementary file 2***. (**B**) Summary of the cerebellar results coming from the modelling. (1) and (2) refer to the models depicted in ***Figure 1***. (**C**) Tau seems to change compartments in the thalamus with age, going from neuronal-like compartments (low sphere fraction) to glial-like compartments (high sphere fraction), also indicated by its important signal drop with age. It suggests that Tau is a marker of neuronal maturation. Its concentration remains high up to postnatal day 30 (P30) in the cerebellum. Tau properties in the cerebellum (decreasing sphere fraction + relatively low sphere fractions) and contrast with the thalamus suggest that Tau could be a marker of cerebellar neuronal development.

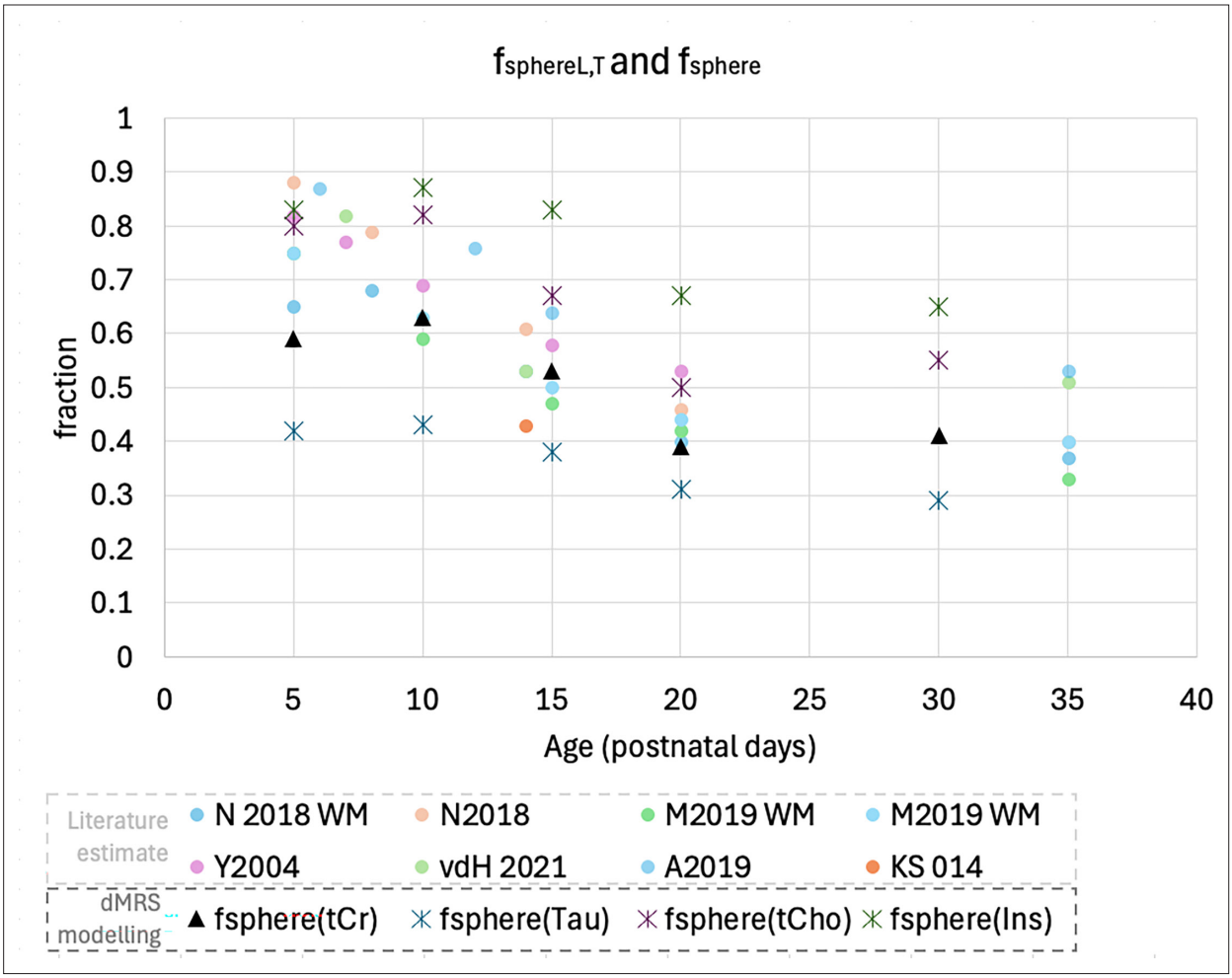

Figure 5—figure supplement 1. Literature estimate of $f_{sphereL,T}$ (as described in ***Supplementary file 2***, pale rounds on the graph) as a function of age compared to f_{sphere}(tCr) (black triangles) f_{sphere}(Tau, tCho, Ins) (stars). Postnatal day 35 (P35) represents any age >P30. Legend: N2018 = ***Nakayama et al., 2018***; M2019 = ***Miterko et al., 2019***; Y2004 = ***Yamanaka et al., 2004***; vdH2021 = ***van der Heijden and Sillitoe, 2021***; A2019 = ***Araujo et al., 2019***; KS2014=***Kim and Scott, 2014***. 'WM' indicates that the estimate included WM.

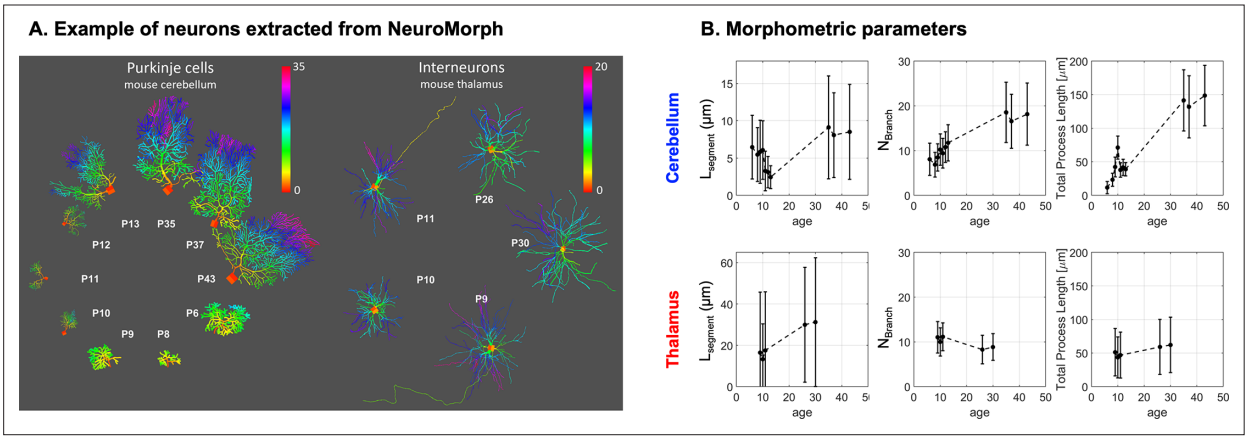

Figure 6. Morphometric parameters extracted from mouse real cells 3D reconstructions on NeuroMorph show a decrease of $L_{segment}$ up to P13 in developing cerebellar Purkinje cells, but not in developing thalamic interneurons. (**A**) Examples of cells extracted from NeuroMorph. The total number of cells used per age and region is given in ***Supplementary file 3***. References: cerebellum P6-P10 (***Fukumitsu et al., 2016***), P10-P13 (***Jayabal et al., 2017***), P35-P43 (***Chen et al., 2013***), thalamus P9-P30 (***Hetsch et al., 2022***). (**B**) The values of branch length (Lsegment), branching order, and total process length are directly estimated from the morphology using the function stat_tree in the Trees MATLAB toolbox.